Silver thiocyanate treatment-induced defect annihilation for enhancement of photoluminescence efficiency of $CsPbBr_3$ perovskite quantum dots

Ho-Young Kim,[1] Seung-Beom Cho,[1] Bo Hou,[2*] and Il-Kyu Park[1*]

[1)]Department of Materials Science and Engineering Seoul National University of Science and Technology, Seoul, 01811, Republic of Korea
[2)]Department of Physics and Astronomy, Cardiff University, Cardiff CF24 3AA, United Kingdom

*Corresponding author. Tel.: +82029706349, fax: +82029706657
e-mail address: HouB6@cardiff.ac.uk (B. Hou), pik@seoultech.ac.kr (I. K. Park)

Abstract. Cesium lead halide perovskite nanostructures have been achieved much attention for many optoelectronic devices, such as solar cells, light-emitting diodes, photodetectors, and sensors due to their sharp emission spectrum, adjustable wide optical bandgap, and high distinct color. However, low emission efficiency and stability still impede their development and application. This paper reports a facile surface modification of the $CsPbBr_3$ quantum dots (QDs) to enhance the optical performance by using a silver thiocyanate (AgSCN) additive. Structural and chemical investigations showed that the QD morphology and size did not change significantly while the SCN was incorporated into the $CsPbBr_3$ QDs with increasing the AgSCN content. In addition, the SCN interacts with Pb in the $CsPbBr_3$ QDs, which indicates that the SCN fills out the Br vacancy site or substitutes the Br anion without significantly affecting the ligand configuration. Therefore, the photoluminescence (PL) intensity and stability of the AgSCN-treated $CsPbBr_3$ QDs were improved compared to the pristine one because the AgSCN acted a critical role in recovering the appropriate surface stoichiometry and eliminating the surface defective sites.

Key words: $CsPbBr_3$; Photoluminescence; Pseudo halide; Quantum dots

*Corresponding authors. E-mail address: HouB6@cardiff.ac.uk (B. Hou), pik@seoultech.ac.kr (I. K. Park)

1. Introduction

Semiconductor quantum dots (QDs) have been achieved much attention because of their importance as a functional building block providing potential opportunities for optoelectronic device applications as well as for surveying novel quantum effects [1,2]. Recently, metal halide perovskite QD structures have considerably attracted attention in display applications due to their superior properties, such as unique exciton binding energy, band structure with defect tolerance for high photoluminescence (PL) efficiency, very narrow PL for high color purity, and wide range of bandgap energy controllability covering the whole visible wavelength spectral range [3-9]. Among the halide-based perovskite alloys, the cesium lead halide perovskite ($CsPbX_3$; X=Cl, Br, and I) based QDs have been investigated widely because of a simple solution process as well as many advantages mentioned above [3-5]. Nevertheless, the intrinsically unstable nature of $CsPbBr_3$ QD structures that deteriorate emission efficiency and stability due to the surface halide defects in air atmospheres are still considered to be a serious problem for practical applications [10-15]. Typically, the deterioration caused by moisture in the surface defects results in a decrease in exciton recombination efficiency and a decrease in emission characteristics [10-15]. To circumvent these problems, many researches have been reported to improve the PL efficiency and stability of $CsPbBr_3$ QDs by introducing novel strategies, such as controlling the surface states, doping foreign elements, constructing core-shell structure, and inducing ligand exchange [16-21]. Among these methods, the ligand exchange strategy has provided an efficient and simple way to improve the stability and luminescence efficiency simultaneously. The surface passivation of $CsPbBr_3$ QDs has been known to be very effective in enhancing the emission efficiency of QD itself because the existence of halide vacancy is one of the major factors restricting the performance of QD emitters. The exchanged ligands can passivate grain boundaries, which

reduces the nonradiative recombination at the surfaces of the QDs and improves their electronic properties. Recently, it has been demonstrated that the surface defects of perovskite QDs are remarkably suppressed by introducing inorganic materials, such as $ZnBr_2$, sodium thiocyanate (NaSCN), NH_4SCN, $Ga(NO_3)$, and LiBr, revealing the important role of QD surface engineering [22-27]. In addition, the emission efficiency and stability of the $CsPbBr_3$ nanostructures were improved by exchanging the organic ligand by the addition of the didodecyldimethyl-ammonium bromide (DDAB) [28]. The added DDAB eliminated the surface point defects by additional Br^- anion and substituted the surface ligand by DDA^+ anion. Therefore, the ligand exchange strategy is effective in improving the chemical stability as well as the emission efficiency and needs more investigations. In this study, we suggest a new pseudo-halide-based surface treatment method, to enhance the PL efficiency and stability of $CsPbBr_3$ QDs. Silver thiocyanate (AgSCN) has been investigated as a pseudo-halide additive and proposed an enhancement mechanism based on the structural, chemical, and optical properties.

2. Experimental

2.1. Synthesis of pristine $CsPbBr_3$ QDs and surface modification by AgSCN

In this study, the pristine $CsPbBr_3$ QDs were fabricated based on a ligand-assisted reprecipitation (LARP) method [6,7]. After synthesis of the $CsPbBr_3$ QDs, their surface was modified using AgSCN additives. Figure 1 shows a schematic diagram of the synthetic procedure and surface modification process of the $CsPbBr_3$ QDs by the AgSCN additives. To synthesize the pristine $CsPbBr_3$ QDs, 0.4 mmol of $PbBr_2$ and CsBr was dissolved in 10 ml of N,N-dimethylformamide (DMF) solvent and stirred for 1 hour at room temperature. And then, 600 μl of oleylamine (OAm) was added to the already prepared precursor solution. The mixed precursor

solution was stirred for 1 hour. The precursor solution was filtered through a 0.2 μm polytetrafluoroethylene syringe filter to remove the impurities and undissolved sources, which resulted in a clean precursor solution. To make a crude solution, 8 mL of oleic acid (OA) was added to 80 ml of a toluene solution and stirred vigorously at room temperature for 1 minute. After rapidly injecting 4 ml of the precursor solution into the toluene solution containing OA, the mixed solution was stirred for 20 seconds to obtain the pristine $CsPbBr_3$ QD solution. The synthesized $CsPbBr_3$ QD solution showed strong green emission under UV light as shown in Fig. 1. All the processes were conducted in a tightly controlled Ar-filled glove box to avoid oxygen and water contamination. The crude solution was then centrifuged at 12,000 rpm for 10 minutes to remove the large particles. Methyl acetate and ethyl acetate are added to the remained solution at a volume ratio of 1:1:1 and centrifuged again at 12,000 rpm for 10 minutes to remove the remaining impurities. Didodecyldimetyl ammonium bromide (DDAB, 99%) and OA were added to the precipitated $CsPbBr_3$ QD solution, and the mixture was uniformly dispersed for 1 minute. Finally, the pristine $CsPbBr_3$ QD solution was obtained by dispersing the precipitates into the 800 μl of *n*-octane. The above procedures were carried out twice to obtain 1,600 μl of pristine $CsPbBr_3$ QD solution. The AgSCN was dissolved into the diethyl sulfide with a concentration of 5, 10, 15, and 20 mg/ml. 10 μl of the dissolved AgSCN solutions with different concentrations were added into the 300 μl of pristine $CsPbBr_3$ QD solutions. These samples are labeled as AgSCN-5, -10, -15, and -20, respectively. Here, the AgSCN was added to the $CsPbBr_3$ QDs to investigate the effect of surface passivation by the pseudo-halide, SCN group. As a reference, 10 μl of diethyl sulfide was added into the $CsPbBr_3$ QD solution to confirm the influence of the solvent itself, but there were no changes in the photoluminescence (PL) and UV-visible absorption spectra. The $CsPbBr_3$ QD solutions were spin-coated on the sapphire and glass substrates to fabricate the thin films for the

optical measurements. After spin-coating at 1,500 rpm for 60 seconds, the QD films were annealed at 100 °C for 10 minutes. The $CsPbBr_3$ QD films showed uniform green emission on the sapphire substrate as shown in Fig. 1.

2.2. Characterizations

The optical properties of the $CsPbBr_3$ QDs were examined using PL and UV-visible spectrophotometer (Agilent 8453). PL spectra were measured at room temperature using a 405 nm diode laser and MAYA 2000 spectrophotometer. Structural properties of the $CsPbBr_3$ QDs were performed by X-ray diffraction (XRD, Rigaku D/Max-2500 diffractometer equipped with a Cu $K\alpha$ source) and transmission electron microscopy (TEM; JEOL-2010). Elemental analysis of the QDs was carried out using a TEM equipped with an energy-dispersive X-ray spectrometer (EDS). The chemical bonding states of the $CsPbBr_3$ QDs were investigated by a Fourier-transform infrared (FT-IR, Thermo scientific, NICOLET iS10) spectroscopy.

3. Results and Discussion

Figure 2 presents the optical properties of the $CsPbBr_3$ QDs by the post-treatment of AgSCN as a surface source. To investigate the effect of AgSCN addition on the optical properties of the $CsPbBr_3$ QDs, UV-visible absorption spectroscopy was measured as shown in Fig. 2(a). By adding an AgSCN source, the $CsPbBr_3$ QDs became more bright under 395 nm UV lamp illumination, while the green emission color remained constant, as shown in the inset of Fig. 2. This was also confirmed by the UV-visible absorption spectra, which showed no change in the shape of spectra and absorption edges even with a variation of the AgSCN content. The shape of

the absorption spectra was similar for all the QDs with a steep absorption edge and sharp exciton absorption peak at about 498 nm. The bandgap energy of pristine $CsPbBr_3$ QDs estimated from the absorption edge was about 2.40 eV (516 nm), which is slightly larger than its bulk bandgap energy of 2.32 eV [29]. The increased bandgap energy of pristine $CsPbBr_3$ QDs would be due to the quantum confinement effect [30]:

$$E_{QD} = E_g + \frac{h^2}{8r^2}\left(\frac{1}{m^*_e} + \frac{1}{m^*_h}\right) - \frac{1.8e^2}{4\pi\varepsilon_r\varepsilon_0 r}$$

where E_{QD} and E_g are the lowest excitation energy of the $CsPbBr_3$ QDs and the bandgap of bulk $CsPbBr_3$ (2.32 eV), respectively. r is the radius of the $CsPbBr_3$ QDs, h is Planck's constant, m^*_e is the electron effective mass, m^*_h is the hole effective mass, e the is electron unit charge, ε_r is the relative permittivity of $CsPbBr_3$, and ε_0 is the vacuum permittivity. Therefore, the reduced size (r) of the $CsPbBr_3$ QDs would result in an increase in bandgap energy. As the AgSCN is added, the main absorption starts to increase at a similar wavelength to the pristine one. In addition, it should be noted that all QDs showed the absorption peak corresponding to the exciton state even with increasing the AgSCN content. This indicates the uniform size distribution. To evaluate the optical emission properties of the AgSCN-treated $CsPbBr_3$ QD films, steady-state PL spectra were measured at room temperature, as shown in Fig. 2(b). The PL spectra of the $CsPbBr_3$ QDs exhibited similar symmetric emission peaks centered around 512 nm while showing different emission intensity and peak positions with increasing the AgSCN. As shown in Fig. 2(c), the PL intensity increased and the emission peak position showed a red-shift with increasing the AgSCN content. This would be due to the substitution of SCN^- pseudo-halide into the Br^- sites of the $CsPbBr_3$ lattice. It should be noted that the PL intensity of the AgSCN-treated $CsPbBr_3$ QDs improved compared to the DDAB-treated one. The emission performance of $CsPbBr_3$ QDs was

known to be improved using DDAB-treatment due to supplement of steric stabilization [28]. Therefore, the AgSCN-treatment can make up the emission efficiency by another effect than the ligand treatment.

Figure 3 shows the TEM images of the pristine and AgSCN-treated $CsPbBr_3$ QDs. The pristine $CsPbBr_3$ QDs show a uniform cuboidal shape with an average particle size of 10.2 nm. The cuboidal $CsPbBr_3$ QDs exhibit well-defined lattice fringes in the high resolution-TEM (HR-TEM) images, which indicates high crystalline quality. The AgSCN-treated $CsPbBr_3$ QDs showed a similar particle shape and size to the pristine one. In addition, no significant change in QD morphology was observed and the well-defined lattice fringes were maintained even with an increase in the AgSCN content (Figs. 3(b)~(e)). The size of $CsPbBr_3$ QDs was in the range between 10~11 nm even with the variation of the AgSCN content, as shown in Fig. 3(f). This suggests that the AgSCN additive did not affect the crystallographic structure or crystallinity of $CsPbBr_3$ QDs. To observe the variation of elemental distribution by adding the AgSCN, EDS was measured for the AgSCN-10 and -20. As shown in Figs. 3(g) and (h), the AgSCN-treated $CsPbBr_3$ QDs mainly consist of Cs, Pb, and Br. It should be noted that the N and S elements were observed while the Ag element (the arrows shown in the spectra) was not found, even though the AgSCN content was added up to 20 mg/ml. Even though the SCN anion would substitute the Br lattice site or fill out its vacancy site, the Ag is not incorporated but would be expelled from the QDs because the ionic radius of Ag^+ (126 pm) is much different from those of Cs^+ (265 pm) and Pb^{2+} (84 pm) to satisfy the tolerance and octahedral factor of the perovskite structure.

The structural evolution of the AgSCN-treated $CsPbBr_3$ QDs was investigated by XRD, as shown in Fig. 4(a). The XRD patterns of the $CsPbBr_3$ QDs were assigned to the cubic phase (JCPDS No. 18-0346), which the atomic crystal structure is shown in the inset of Fig. 4(a). The

pristine $CsPbBr_3$ and AgSCN-treated $CsPbBr_3$ QDs showed an identical cubic crystal structure without showing any trace of a secondary phase. This indicates that the $CsPbBr_3$ QDs maintained a cubic structure even after the AgSCN-treatment. Even as the AgSCN content was increased from 0 to 20 mg/ml, no additional peak appeared. This reveals an absence of any secondary phase or alloys corresponding to the Ag or SCN related phases. However, the diffraction peaks were shifted to a higher angle side as the AgSCN content was increased from 0 to 15 mg/ml. Figures 4(b) and (c) show the variation of the (200) peak position and full-width at half-maximum (FWHM) of (200) peak according to the AgSCN content. This variation was attributed to the smaller ionic radius of SCN^- than that of Br^-. An SCN^- moiety is a pseudo-halide with a linear shape and an atomic radius of 137 pm, which is smaller than Br^- (196 pm) [31]. As the SCN^- is incorporated by substituting into the Br^- lattice sites or its vacancy site, the unit cell of the AgSCN-treated $CsPbBr_3$ QDs would be shrunk compared with that of the pristine one. This is confirmed from the shifted diffraction peak to the higher angle side, as expected by Bragg's law. As shown in Fig. 4(c), the FWHM of (200) peak decreases with increasing the AgSCN content up to 15 mg/ml, while it increases as the AgSCN content increases further to 20 mg/ml. This indicates that the crystallinity of the $CsPbBr_3$ is improved due to the annihilation of various point defects or microstructural defects by incorporating a small amount of SCN^- anions. This improved stability of $CsPbBr_3$ is attributed to stronger chemical bonding between SCN^- and Pb^{2+} than that between Br^- and Pb^{2+} [31]. Therefore, the AgSCN can improve the stability of $CsPbBr_3$ QDs by eliminating the Br-related vacant sites or substituting the Br lattice sites, which are resulted in improved PL efficiency.

Fourier-transform infrared (FTIR) spectroscopy revealed the modification of surface functional groups on the $CsPbBr_3$ QDs, as shown in Fig. 5. The peaks at 1,378~1,461 and 2,856~2,957 cm^{-1} are corresponding to the functional groups of COO and C-H stretching modes,

respectively. The C-H stretching modes are from the carboxyl acid of the OA ligand. The broad peaks at 2,065~2,087 cm^{-1} found for the AgSCN-treated QDs are corresponding to the SCN functional group [32]. This broad peak is consistent with the C≡N bond of a thiocyanate bound to lead with a Pb−S bond. The position of this peak exhibits a distinctive shift depending on the identity of the atom the thiocyanate is bound to [33]. This indicates that the SCN interacts with Pb in the $CsPbBr_3$ QDs by filling out the Br vacancy site or substituting the Br anion. The SCN-related peak intensity increases as the AgSCN content increases from 0 to 20 mg/ml, while the peaks corresponding to the C-H stretching mode remain constant. This indicates that the addition of AgSCN does not affect the ligand passivation. Therefore, the AgSCN-treatment would passivate the $CsPbBr_3$ QD surface without significantly affecting the ligand configuration.

To investigate the emission stability of the $CsPbBr_3$ QDs, the PL was measured for the QD thin films after two and three weeks stored in air ambient. Figure 6(a) shows the PL spectra measured three weeks later and variation of the normalized PL intensity with time. All the $CsPbBr_3$ QDs show degradation of PL intensity with increasing the aging time in air ambient. Much has been reported about the degradation of PL efficiency of perovskite materials. Two main degradation mechanisms of perovskite nanostructures have been reported as oxidation and surface defect formation. The oxidation of metal cations in perovskite crystal structure occurs as the electrons have been captured by oxygen molecules [11,12]. To circumvent this problem, modifying the surface of perovskite QDs or the strong steric hindrance of surface ligands on the QD surface can greatly improve their stability to oxygen. In addition, the perovskite structure can be easily degraded in a humid environment, because the perovskite materials exhibit ionic bonding [13,14]. Due to moisture induction, surface atoms fall off to cause surface defects, and it is also easy to cause agglomeration, which ultimately reduces quantum yield and affects the luminous

performance [34]. Here, the AgSCN-treatment circumvents these problems by passivating anion vacancy sites and removing excess Pb atoms on the surface of $CsPbBr_3$ QDs as shown in the schematic (Fig. 6(b)). In this way, the AgSCN-treatment acts a critical role in improving the optical performances by recovering the appropriate surface stoichiometry and eliminating the surface defective sites. Therefore, the AgSCN-treatment is effective in improving the emission stability as well as in enhancing the PL efficiency.

4. Conclusion

In summary, we report the enhancement of PL efficiency and stability of green light-emitting $CsPbBr_3$ QDs based on the post-treatment of AgSCN. As the AgSCN content increased, no significant change in QD morphology and size was observed by TEM investigations. However, the XRD and EDS results showed that the SCN was incorporated into the $CsPbBr_3$ QDs while the crystalline structure was maintained consistently even with increasing the AgSCN content. The FTIR results show that the SCN interacts with Pb in the $CsPbBr_3$ QDs, which indicates that the SCN fills out the Br vacancy site or substitutes the Br anion without significantly affecting the ligand configuration. The PL intensity and stability of the AgSCN-treated $CsPbBr_3$ QDs were improved compared to the pristine one. Based on the structural and chemical investigations about the AgSCN-treated $CsPbBr_3$ QDs, the emission efficiency enhancement mechanism was suggested. The AgSCN acted a critical role in recovering the appropriate surface stoichiometry and eliminating the surface defective sites to improve the optical performances of the $CsPbBr_3$ QDs. This enhancement strategy can be applied to a wide variety of QD materials to improve their optical performances for optoelectronic device applications.

Acknowledgments

This study was supported by the Research program funded by the Seoultech (Seoul National University of Science & Technology)

References

[1] C.R. Kagan, L.C. Bassett, C.B. Murray, S.M. Thompson, Colloidal quantum dots as platforms for quantum information science, Chem. Rev. 121 (2021) 3186–3233.

[2] B. Li, M. Lu, J. Feng, J. Zhang, P.M. Smowton, J.I. Sohn, I.K. Park, H. Zhong, B. Hou, Colloidal quantum dot hybrids: an emerging class of materials for ambient lighting, J. Mater. Chem. C 8 (2020) 10676.

[3] L. Protesescu, S. Yakunin, M.I. Bodnarchuk, F. Krieg, R. Caputo, C.H. Hendon, R.X. Yang, A. Walsh, M.V. Kovalenko, Nanocrystals of cesium lead halide perovskites ($CsPbX_3$, X = Cl, Br, and I): Novel optoelectronic materials showing bright emission with wide color gamut, Nano Lett. 15 (2015) 3692−3696.

[4] D.K. Sharma, S. Hirata, M. Vacha, Single-particle electroluminescence of $CsPbBr_3$ perovskite nanocrystals reveals particle-selective recombination and blinking as key efficiency factors. Nat. Commun. 10 (2019) 4499.

[5] L.N. Quan, F.P. García de Arquer, R.P. Sabatini, E.H. Sargent, Perovskites for light emission. Adv. Mater. 30 (2018) 1801996.

[6] S.B. Cho, J.I. Sohn, S.S. Lee, S.G Moon, B. Hou, I.K. Park, Colour-encoded electroluminescent white light-emitting diode enabled by perovskite-Cu-In-S quantum composites, J. Mater. Chem. C 9 (2021) 7027−7034.

[7] S.G. Moon, S.B. Cho, K.K. Kim, I.K. Park, Mixed halide $CsPb(Br_{1-x}I_x)_3$ nanocrystals for green, orange, and red light-emitting diodes, J. Alloys Comp. 858 (2021) 157643.

[8] S.B. Cho, J.W. Jung, Y.S. Kim, C.H. Cho, I.K. Park, Emission wavelength control of $CsPb(Br_{1-x}Cl_x)_3$ nanocrystals for blue light-emitting diode applications, CrystEngComm 23 (2021) 2746−2755.

[9] Y. Li, J. Feng, H. Sun, Perovskite quantum dots for light-emitting devices, Nanoscale 11 (2019) 19119−19139.

[10] Z. Shi, S. Li, Y. Li, H. Ji, X. Li, D. Wu, T. Xu, Y. Chen, Y. Tian, Y. Zhang, C. Shan, G. Du, Strategy of a solution-processed all-inorganic heterostructure for humidity/temperature-stable perovskite quantum dot light-emitting diodes, ACS Nano 12 (2018) 1462−1472.

[11] N. Aristidou, I. Sanchez-Molina, T. Chotchuangchutchaval, M. Brown, L. Martinez, T. Rath, S.A. Haque, The role of oxygen in the degradation of methylammonium lead trihalide perovskite photoactive layers, Angew. Chem. Int. Ed. 54 (2015) 8208–8212.

[12] M. Lorenzon, L. Sortino, Q. Akkerman, S. Accornero, J. Pedrini, M. Prato, V. Pinchetti, F. Meinardi, L. Manna, S. Brovelli, Role of nonradiative defects and environmental oxygen on exciton recombination processes in $CsPbBr_3$ perovskite nanocrystals, Nano Lett. 17 (2017) 3844–3853.

[13] S. Pathak, A. Sepe, A. Sadhanala, F. Deschler, A. Haghighirad, N. Sakai, K.C. Goedel, S.D. Stranks, N. Noel, M. Price, Atmospheric influence upon crystallization and electronic disorder and its impact on the photophysical properties of organic-inorganic perovskite solar cells, ACS Nano 9 (2015) 2311–2320.

[14] G.E. Eperon, S.N. Habisreutinger, T. Leijtens, B.J. Bruijnaers, J.J. van Franeker, D.W. DeQuilettes, S. Pathak, R.J. Sutton, G. Grancini, D.S. Ginger, The importance of moisture in hybrid lead halide perovskite thin film fabrication, ACS Nano 9 (2015) 9380–9393.

[15] L. Zhang, M.G. Ju, W. Liang, The effect of moisture on the structures and properties of lead halide perovskites: A first-principles theoretical investigation, Phys. Chem. Chem. Phys. 18 (2016) 23174–23183.

[16] C. Zheng, C. Bi, F. Huang, D. Binks, J. Tian, Stable and strong emission $CsPbBr_3$ quantum dots by surface engineering for high-performance optoelectronic films, ACS Appl. Mater. Interfaces 11 (2019) 25410–25416.

[17] M. Zirak, E. Moyen, H. Alehdaghi, A. Kanwat, W.C. Choi, J. Jang, Anion- and cation-codoped all-inorganic blue-emitting perovskite quantum dots for light-emitting diodes, ACS Appl. Nano Mater. 2019, 2, 9, 5655–5662.

[18] M. Zhang, Z.Q. Tian, D.L. Zhu, H. He, S.W. Guo, Z.L. Chen, D.W. Pang, Stable $CsPbBr_3$ perovskite quantum dots with high fluorescence quantum yields, New J. Chem. 42 (2018) 9496–9500.

[19] F. Boussoufi, M. Pousthomis, A. Kuntzmann, M. D'Amico, G. Patriarche, B. Dubertret, Spray-drying polymer encapsulation of $CsPbBr_3$ perovskite nanocrystals with enhanced photostability for LED downconverters, ACS Appl. Nano Mater. 4 (2021) 7502–7512.

[20] L. Xu, J. Li, T. Fang, Y. Zhao, S. Yuan, Y. Dong, J. Song, Synthesis of stable and phase-adjustable $CsPbBr_3$@Cs_4PbBr_6 nanocrystals via novel anion–cation reactions, Nanoscale Adv. 1 (2019) 980–988.

[21] H. Yang, W. Yin, W. Dong, L. Gao, C.H. Tan, W. Li, X. Zhang, J. Zhang, Enhancing the light-emitting performance and stability in $CsPbBr_3$ perovskite quantum dots via simultaneous doping and surface passivation, J. Mater. Chem. C (2020), 8, 14439–14445.

[22] S. Sun, M. Lu, J. Guo, F. Zhang, P. Lu, Y. Fu, X. Bai, Z. Shi, Z. Wu, W.W. Yu, Y. Zhang, $ZnBr_2$ mediated transformation from nonluminescent Cs_4PbBr_6 to green-emitting Zn-doped

$CsPbBr_3/Cs_4PbBr_6$ nanocrystals for electroluminescent light-emitting diodes, Chem. Eng. J. 433 (2022) 133556.

[23] T. Wu, J. Li, Y. Zou, H. Xu, K. Wen, S. Wan, S. Bai, T. Song, J. A. McLeod, S. Duhm, F. Gao, B. Sun, High-performance perovskite light-emitting diode with enhanced operational stability using lithium halide passivation, Angew. Chem. Int. Ed. 59 (2020) 4099–4105.

[24] J. Wang, Y. Xu, S. Zou, C. Pang, R. Cao, Z. Pan, C. Guo, S. Hu, J. Liu, Z. Xie, Z. Gong, Effective defect passivation of $CsPbBr_3$ quantum dots using gallium cations toward the fabrication of bright perovskite LEDs, J. Mater. Chem. C 9 (2021) 11324–11330.

[25] M. Lu, J. Guo, P. Lu, L. Zhang, Y. Zhang, Q. Dai, Y. Hu, V. L. Colvin, W.W. Yu, Ammonium thiocyanate-passivated $CsPbI_3$ perovskite nanocrystals for efficient red light-emitting diodes, J. Phys. Chem. C 123 (2019) 22787–22792.

[26] D. Yoo, J. Y. Woo, Y. Kim, S. W. Kim, S.-H. Wei, S. Jeong, Y.-H. Kim, Origin of the stability and transition from anionic to cationic surface ligand passivation of all-inorganic cesium lead halide perovskite nanocrystals, J. Phys. Chem. Lett. 11 (2020) 652–658.

[27] J.B. Cho, S.B. Cho, I.K. Park, Performance enhancement of $CsPbBr_3$ thin film-based light-emitting diodes by CsF-induced surface modification, J. Alloys Comp. 891 (2022) 161996.

[28] J. Pan, L. Quan, Y. Zhao, W. Peng, B. Murali, S.P. Sarmah, M. Yuan, L. Sinatra, N.M. Alyami, J. Liu, E. Yassitepe, Z. Yang, O. Voznyy, R. Comin, M.N. Hedhili, O.F. Mohammed, Z.H. Lu, D. Kim, E.H. Sargent, O.M. Bakr, Highly efficient perovskite quantum-dot light emitting diodes by surface engineering, Adv. Mater. 28 (2016) 8718.

[29] M. Sebastian, J.A. Peters, C.C. Stoumpos, J. Im, S.S. Kostina, Z. Liu, M.G. Kanatzidis, A.J. Freeman, B.W. Wessels, Excitonic emissions and above-band-gap luminescence in the single-crystal perovskite semiconductors $CsPbBr_3$ and $CsPbCl_3$, Phys. Rev. B 92 (2015) 235210.

[30] L.E. Brus, Electron-electron and electron-hole interactions in small semiconductor crystallite: The size dependence of the lowest excited electronic state, J. Chem. Phys. 80 (1984) 4403.

[31] P. Suksaengrat, N. Faibut, A. Chompoosor, Influence of an SCN^- moiety on the electronic properties of γ-$CsPb(SCN)_xBr_{3-x}$ and the performance of carbon-based HTL-free γ-$CsPb(SCN)_xBr_{3-x}$ perovskite solar cells, J. Mater. Sci.: Mater. Electron. 32 (2021) 1557–1569.

[32] M. Hou, A. Yu, R. Lu, Effects of HPO_4^{2-} and SCN^- on the hydrogen bond network of water: femtosecond OHD-RIKES and FTIR measurements, J. Raman Spectrosc. 48 (2016) 108–112.

[33] B.A. Koscher, J.K. Swabeck, N.D. Bronstein, A.P. Alivisatos, Essentially trap-free $CsPbBr_3$ colloidal nanocrystals by postsynthetic thiocyanate surface treatment, J. Am. Chem. Soc. 139 (2017) 6566−6569.

[34] L. Zhang, M.G. Ju, W. Liang, The effect of moisture on the structures and properties of lead halide perovskites: A first-principles theoretical investigation. Phys. Chem. Chem. Phys. 18 (2016) 23174–23183.

Figure captions

Figure 1. The schematic synthesis process of $CsPbBr_3$ QDs by post-treatment of AgSCN.

Figure 2. (a) UV-vis absorption spectra of $CsPbBr_3$ QD solutions with the variation of AgSCN additive content. The emission images of the QD solutions were taken under excitation by a commercial UV lamp. (b) PL spectra and emission images of $CsPbBr_3$ QD films coated on sapphire substrate with the variation of AgSCN additive content. The PL was taken under excitation by a 405 nm laser. (c) Variation of the PL emission peak emission energy and integrated intensity of the $CsPbBr_3$ QD films with the variation of AgSCN content.

Figure 3. TEM image of synthesized $CsPbBr_3$ QDs; (a) pristine $CsPbBr_3$ QDs, (b) 5 mg/mL of AgSCN-treated, (c) 10 mg/mL of AgSCN-treated, (d) 15 mg/mL of AgSCN-treated, (e) 20 mg/mL of AgSCN-treated $CsPbBr_3$ QDs. (f) Variation of the average size of $CsPbBr_3$ QDs with the variation of AgSCN content. EDS spectra of (g) 10 mg/mL of AgSCN-treated and (h) 20 mg/mL of AgSCN-treated $CsPbBr_3$ QDs.

Figure 4. (a) Normalized XRD patterns of the $CsPbBr_3$ QDs with the variation of AgSCN content. The inset shows the crystal structure of the cubic $CsPbBr_3$ phase. (b) Variation of (200) peak of the $CsPbBr_3$ QDs with the variation of AgSCN content. (c) The variation of (200) diffraction peak position and its FWHM with the variation of AgSCN content.

Figure 5. (a) Normalized FTIR spectra of the $CsPbBr_3$ QDs with the variation of AgSCN content. (b) Variation of FTIR peaks corresponding to SCN bonding.

Figure 6. (a) PL spectra and emission images of $CsPbBr_3$ QD films after three weeks later in the air. The inset shows the variation of normalized integrated PL intensity with time. (b) Schematics of microstructural evolution showing the modified QD surface after the DABB and AgSCN treatments.

Figures

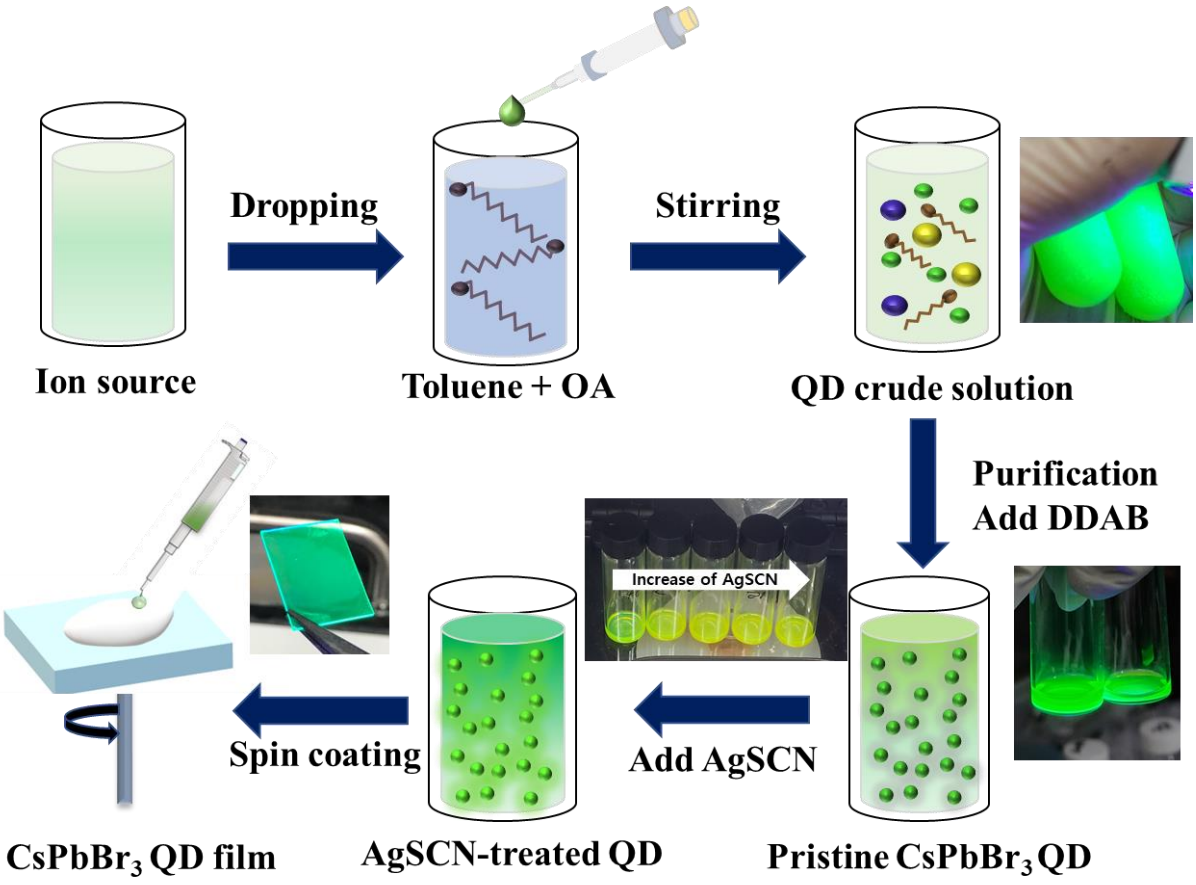

Figure 1 of 6. H. Y. Kim *et al.*

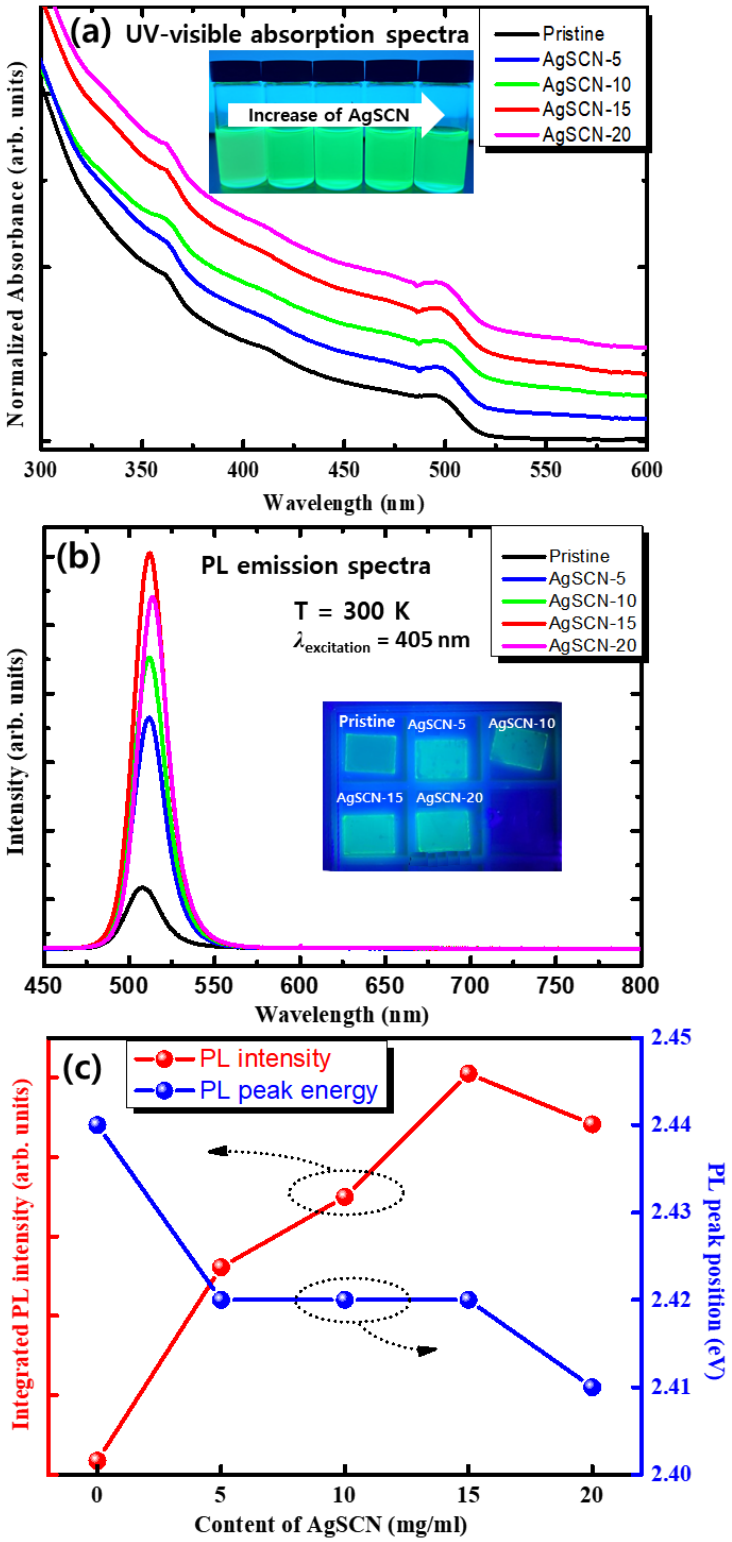

Figure 2 of 6. H. Y. Kim *et al.*

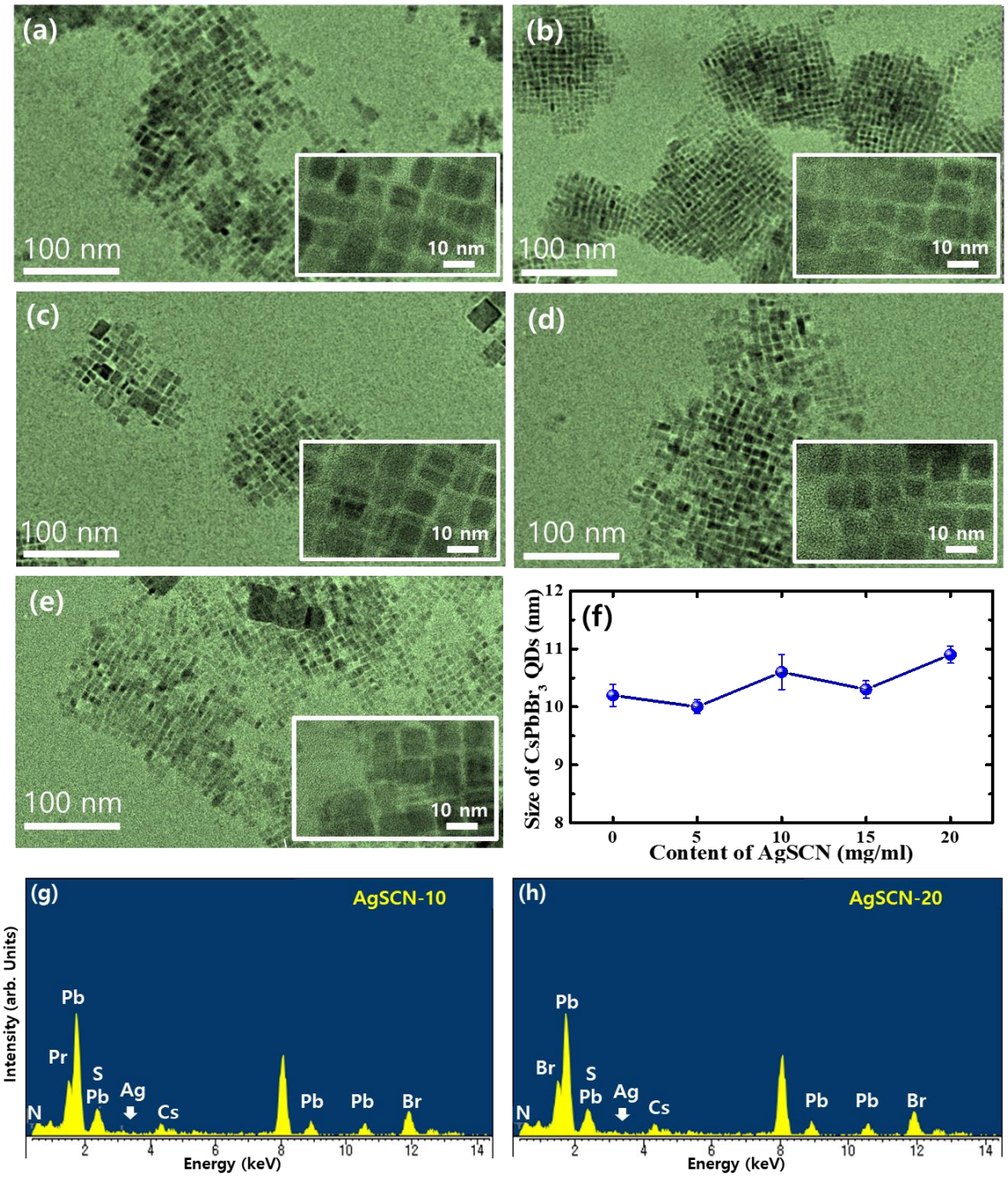

Figure 3 of 6. H. Y. Kim *et al.*

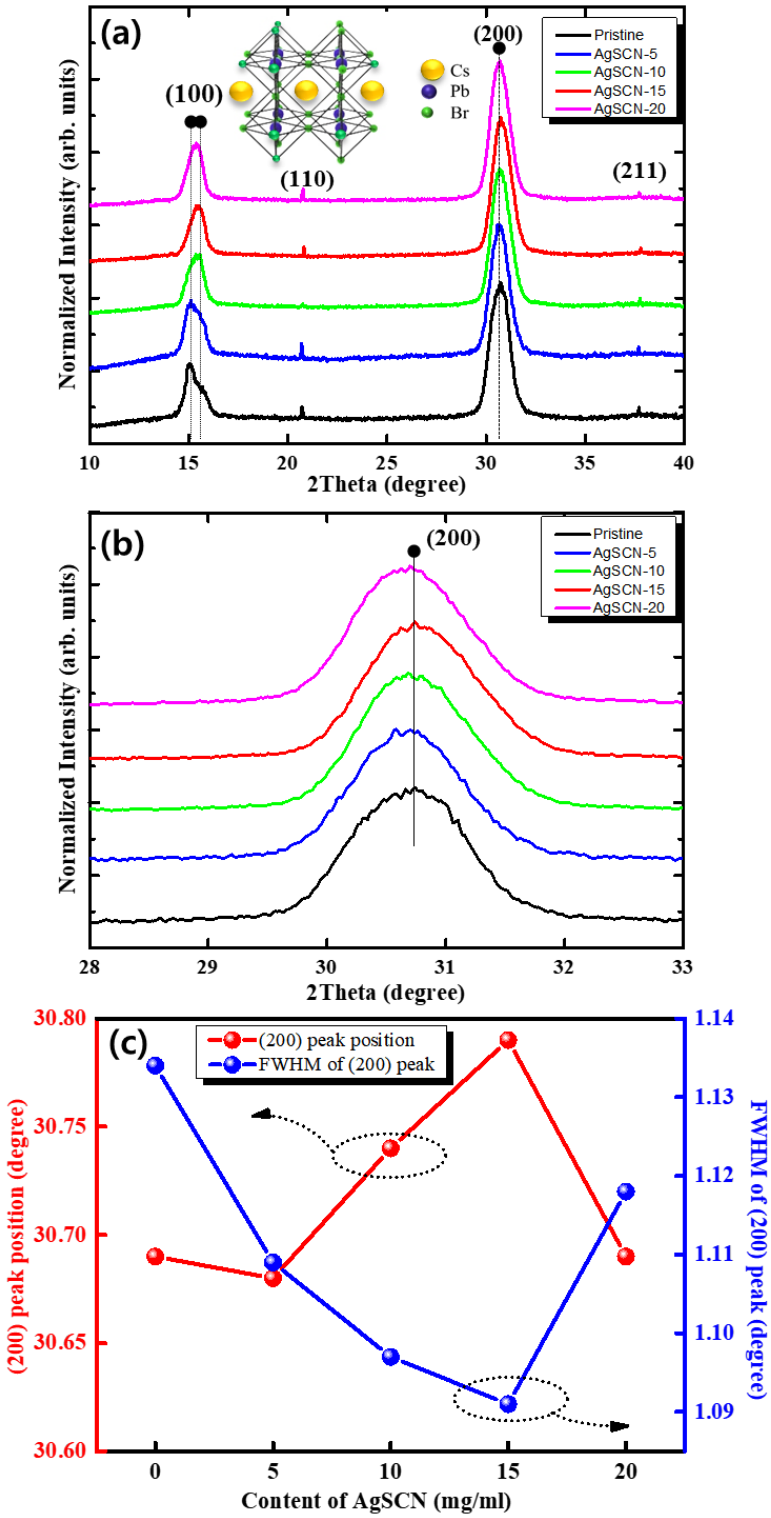

Figure 4 of 6. H. Y. Kim *et al.*

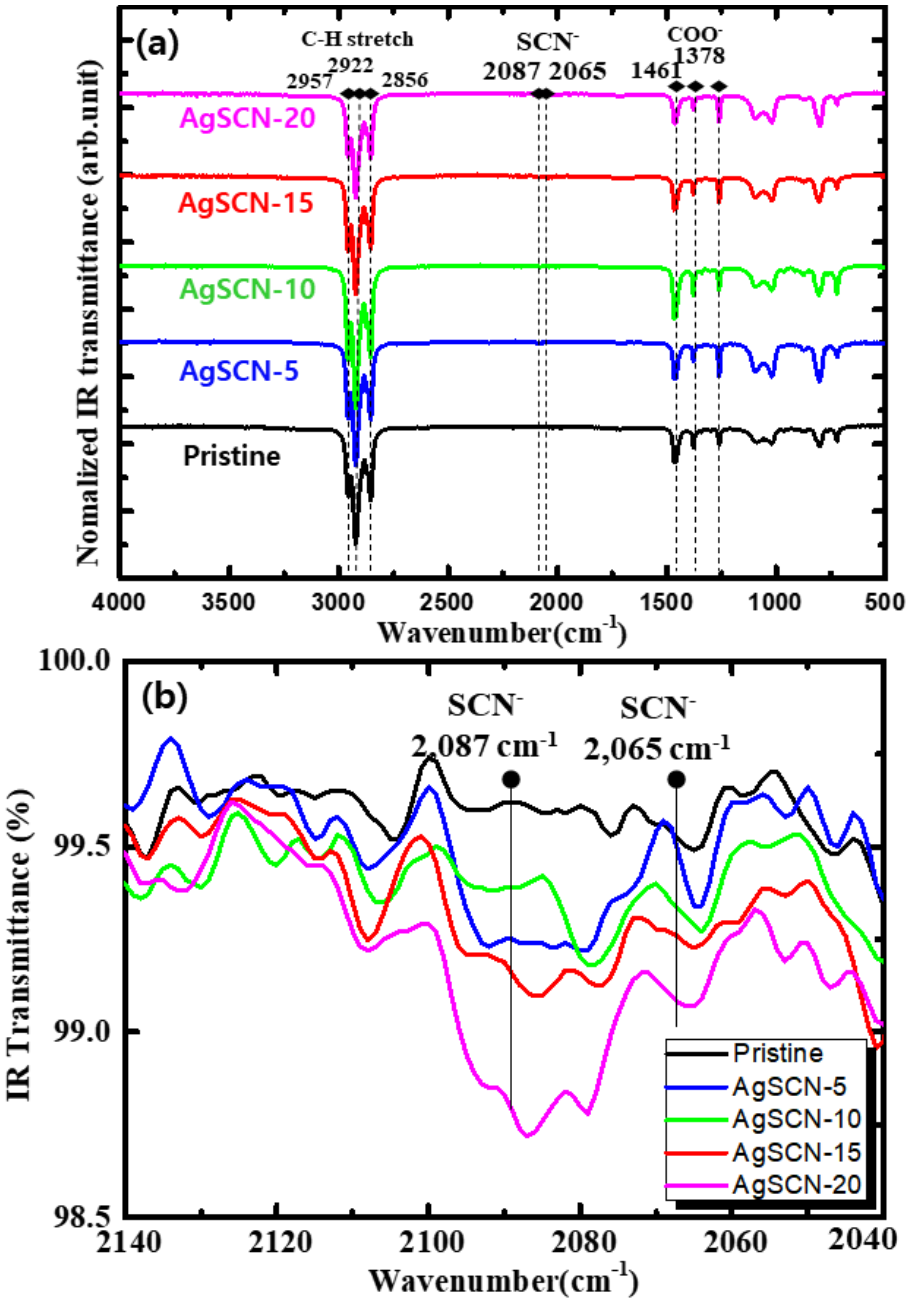

Figure 5 of 6. H. Y. Kim *et al.*

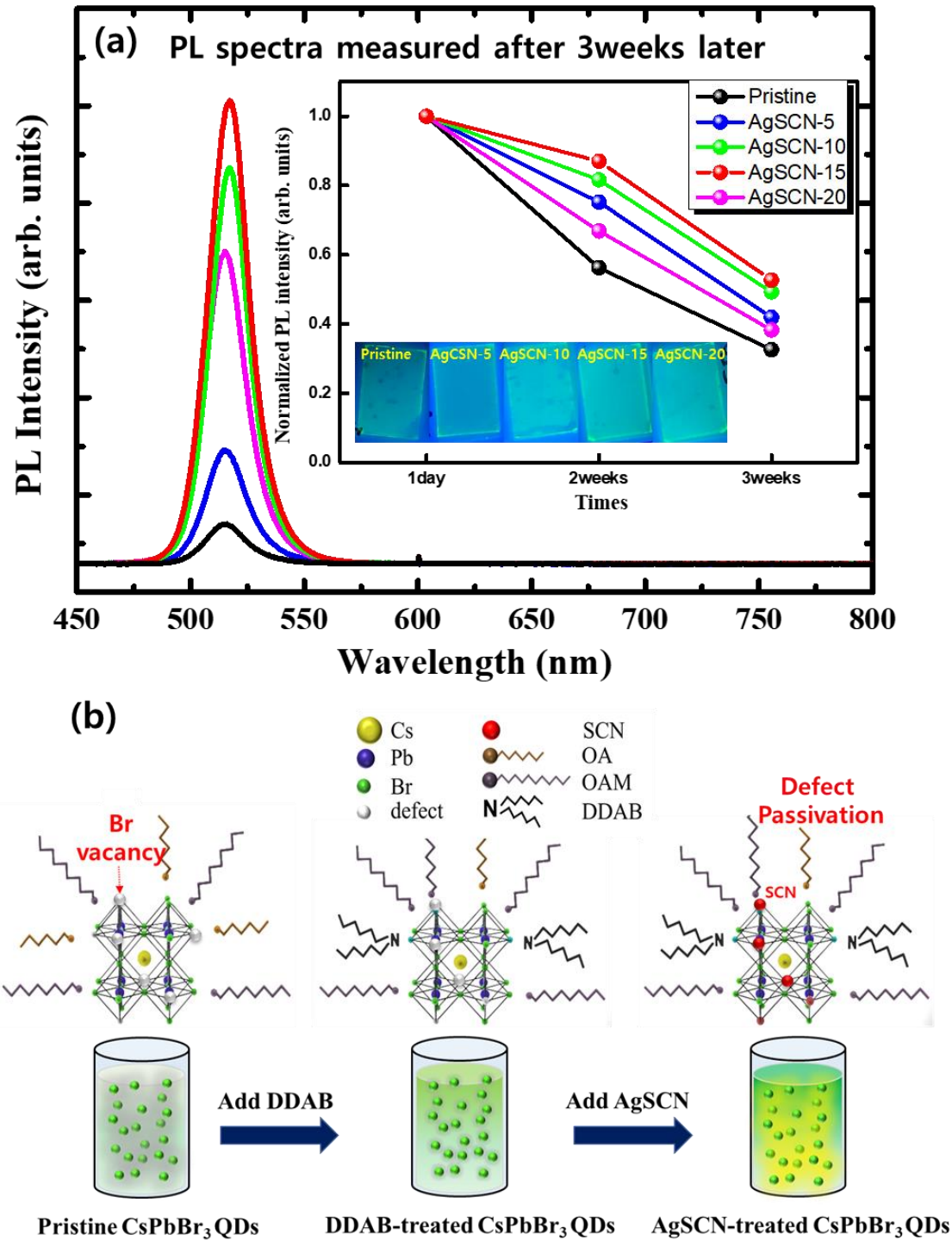

Figure 6 of 6. H. Y. Kim *et al.*